



HAL
open science

Monochromatic internal waves: from theory to experiment

B. Voisin

► **To cite this version:**

B. Voisin. Monochromatic internal waves: from theory to experiment. 18ème Congrès Français de Mécanique, Aug 2007, Grenoble, France. pp.1346. hal-00268819v1

HAL Id: hal-00268819

<https://hal.science/hal-00268819v1>

Submitted on 31 Mar 2011 (v1), last revised 5 Apr 2011 (v2)

HAL is a multi-disciplinary open access archive for the deposit and dissemination of scientific research documents, whether they are published or not. The documents may come from teaching and research institutions in France or abroad, or from public or private research centers.

L'archive ouverte pluridisciplinaire **HAL**, est destinée au dépôt et à la diffusion de documents scientifiques de niveau recherche, publiés ou non, émanant des établissements d'enseignement et de recherche français ou étrangers, des laboratoires publics ou privés.

Monochromatic internal waves: from theory to experiment

Bruno Voisin

Laboratoire des Écoulements Géophysiques et Industriels, CNRS, UJF, INPG
BP 53, 308041 Grenoble Cedex 9; Bruno.Voisin@hmg.inpg.fr

Abstract :

An analytical theory is presented for the generation of small-amplitude three-dimensional monochromatic internal waves by an oscillating object. The theory expresses the structure of the waves in terms of the size of the object, the viscosity of the fluid and the time elapsed since the start-up; to this, it adds near-field effect and modification of the added mass of the object by the stratification. Comparison with experiment allows assessment of the relative importance of all five effects.

Key-words :

internal waves; stratified fluids

1 Introduction

Interest in the generation of monochromatic internal waves has recently been revived, owing on one hand to the realization of the importance of internal tides for mixing the ocean (St Laurent and Garrett, 2002), and on the other hand to the advent of digital measurement techniques such as synthetic Schlieren and Particle Image Velocimetry (Dalziel et al., 2000).

Most laboratory experiments so far have dealt with two-dimensional situations, and the agreement with theory has been found satisfactory; see for example Sutherland et al. (1999) for a vertically oscillating cylinder. Lately, tomographic inversion has allowed the generalization of synthetic Schlieren to three-dimensional axisymmetric situations (Onu et al., 2003), a generalization applied by Flynn et al. (2003) to a vertically oscillating sphere. In doing so, a discrepancy between experiment and theory has been revealed.

The present paper proposes amendments to the theory, in order to remove the discrepancy. Three effects are considered: interference with transients produced by the start-up of the motion; near field; modification of the added mass of the oscillating object by the stratification. The exposition is focused on the comparison with Flynn et al. (2003); the details of the theory will be presented elsewhere (Voisin, 2007a, b).

2 The classical theory revisited

In a uniformly stratified fluid of buoyancy frequency N , an object of characteristic radius a generates monochromatic internal waves by oscillating at frequency $\omega < N$ with surface velocity $\mathbf{U}(\mathbf{x})e^{-i\omega t}$. The waves vary with time through the factor $e^{-i\omega t}$, which is implicit in the following. Wave beams are formed, on a double cone of vertical axis, apex at the object and semi-angle $\theta = \arccos(\omega/N)$. Conical polar coordinates $(x_{\pm}, \varphi, z_{\pm})$ are introduced, with φ the azimuthal angle, $\pm z_{\pm}$ the direction of energy propagation and x_{\pm} the direction of phase propagation. In terms of the cylindrical polar coordinates (r_h, φ, z) , we have

$$x_{\pm} = r_h \cos \theta \mp z \sin \theta, \quad z_{\pm} = \pm r_h \sin \theta + z \cos \theta. \quad (1)$$

The coordinates (x_+, φ, z_+) are used in the upper half-space $z > 0$ and the coordinates (x_-, φ, z_-) in the lower half-space $z < 0$, so that $\pm = \text{sign } z$.

2.1 Calculation of the waves

The classical approach to this problem dates back to Lighthill (1978, §4.10): the oscillating object is represented by a source term in the wave equation, say, a source of mass releasing the volume $q(\mathbf{x})$ of fluid per unit volume per unit time, and the waves are calculated in the far field. An integral over the transverse wavenumber k_{\pm} is obtained. However, this integral diverges along the wave rays tangent to the surface of the object. Viscosity comes into play (Lighthill, 1978, §4.10), attenuating each Fourier component at the rate βk_{\pm}^3 per unit distance along rays, with ν the kinematic viscosity and

$$\beta = \frac{\nu}{2\omega \tan \theta}. \quad (2)$$

Unsteadiness comes into play as well (Voisin, 2003), preventing, at time t after impulsive start-up, each Fourier component to travel further than a distance $1/(\alpha k_{\pm})$ along rays, with

$$\alpha = \frac{1}{\omega t \tan \theta}. \quad (3)$$

The velocity disturbance becomes (Voisin 2007a)

$$\mathbf{u} \sim \pm \frac{\mathbf{e}_{z_{\pm}}}{2^{5/2} \pi^{3/2}} \left(\frac{\cot \theta}{|z_{\pm}|} \right)^{1/2} e^{-i\pi/4} \int_0^{1/(\alpha|z_{\pm}|)} e^{-\beta k_{\pm}^3 |z_{\pm}|} k_{\pm}^{1/2} q_{\pm}(k_{\pm}, \varphi, 0) e^{ik_{\pm} x_{\pm}} dk_{\pm} \quad (4)$$

with $\mathbf{e}_{z_{\pm}}$ a unit vector along the z_{\pm} -axis and $q_{\pm}(k_{\pm}, \varphi, m_{\pm}) = q(\mathbf{k})$. Hereinafter the definition of Fourier transforms is $f(\mathbf{k}) = \int f(\mathbf{x}) \exp(-i\mathbf{k} \cdot \mathbf{x}) d^3k$.

Transitions take place, as the waves propagate away from the source, between a bimodal regime governed by the spectrum of the source and a unimodal regime governed by either viscosity (Makarov et al., 1990) or unsteadiness. The names ‘bimodal’ and ‘unimodal’ refer to the transverse profile of velocity amplitude: a bimodal profile exhibits two peaks on either side of the axis of the wave beam, and a unimodal profile a single peak at this axis. The transitions are illustrated in figure 1. They are characterized by two parameters,

$$\sigma_v = \frac{(\beta|z_{\pm}|)^{1/3}}{a} = \left(\frac{|z_{\pm}|/a}{Re \tan \theta} \right)^{1/3} \quad \text{and} \quad \sigma_u = \frac{\alpha|z_{\pm}|}{a} = \frac{|z_{\pm}|/a}{\omega t \tan \theta}, \quad (5)$$

involving the length scales of the problem, with $Re = 2\omega a^2/\nu$ the Reynolds number. In the (σ_u, σ_v) -plane a transition diagram may be drawn (figure 2), in which the boundary between the bimodal and unimodal zones is defined, for the quantity considered, by the largest distance $|z_{\pm}|$ at which the concavity of the profile at the axis $x_{\pm} = 0$ changes sign.

2.2 Representation of the oscillating object

Since forcing takes place at the surface S of an oscillating object, the most natural representation of this object is a surface distribution of singularities. A popular approximation, dating back to Gorodtsov and Teodorovich (1986) and Makarov et al. (1990), consists in borrowing the distribution from the theory of homogeneous fluids, on the assumption that, for small amplitude of oscillation A compared with the radius a of the object, the influence of the stratification is negligible in the vicinity of the object. For a rigid sphere of radius a oscillating at the velocity \mathbf{U} , the approximation yields

$$q(\mathbf{x}) = \frac{3}{2} \mathbf{U} \cdot \frac{\mathbf{x}}{r} \delta(r-a), \quad q(\mathbf{k}) = -6i\pi a^2 \mathbf{U} \cdot \frac{\mathbf{k}}{\kappa} j_1(\kappa a), \quad (6)$$

with $r = |\mathbf{x}|$ and $\kappa = |\mathbf{k}|$, and $j_1(x) = (\sin x)/x^2 - (\cos x)/x$ a spherical Bessel function.

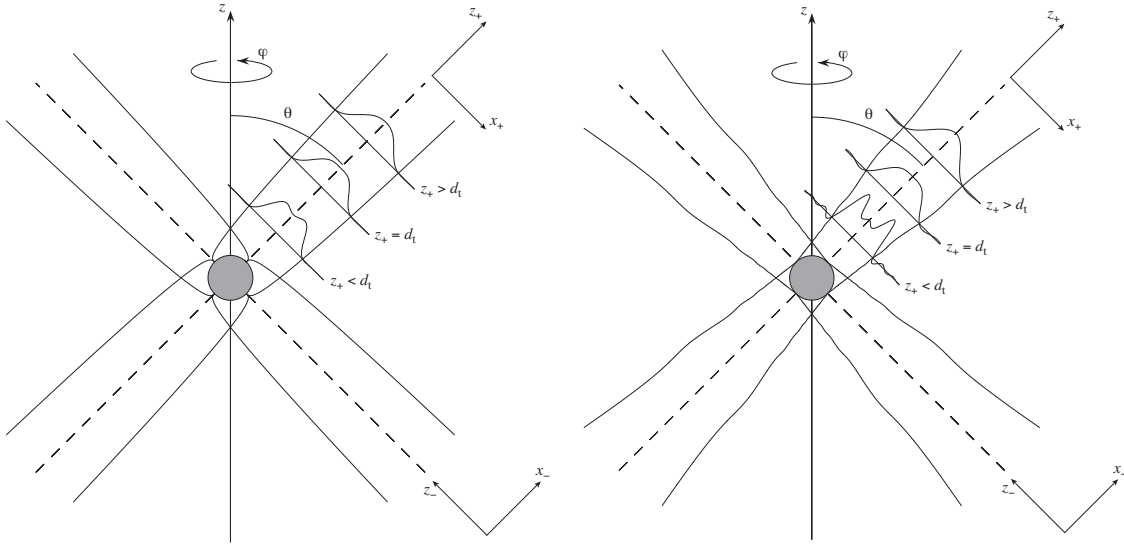


FIG. 1 – Wave beams from a pulsating sphere, accounting for either viscous effects at $Re = 283$ (left) or unsteady effects at $\omega t = 21$ (right). The wave intensity profile is drawn at three distances z_+ from the sphere, respectively before, at and after the transition from bimodality to unimodality at distance d_t . Distances are drawn to scale with respect to the size of the sphere.

3 Beyond the classical theory

3.1 Near-field effects

In the classical approach, neither Lighthill's far-field approximation nor its viscous and unsteady extension (4) have their conditions of validity specified. Going back to the wave equation, and assuming large time $\omega t \gg 1$ and large Reynolds number $Re \gg 1$ but leaving r/a arbitrary, we obtain (Voisin 2007a)

$$\mathbf{u} \sim \pm \frac{\cos \theta}{8\pi^2} \int_0^{2\pi} d\varphi_k \mathbf{e}_{m_{\pm}}(\varphi_k) \int_0^{\cos \theta / (\alpha |z|)} dk_{\pm} e^{-\beta k_{\pm}^3 |z| / \cos \theta} k_{\pm} q_{\pm}(k_{\pm}, \varphi_k, 0) e^{ik_{\pm} \Phi(\varphi_k)}, \quad (7)$$

with

$$\Phi(\varphi_k) = r_h \cos \theta \cos(\varphi_k - \varphi) \mp z \sin \theta \quad (8)$$

and

$$\mathbf{e}_{m_{\pm}}(\varphi_k) = \pm \mathbf{e}_{r_h} \sin \theta \cos(\varphi_k - \varphi) \pm \mathbf{e}_{\varphi} \sin \theta \sin(\varphi_k - \varphi) + \mathbf{e}_z \cos \theta. \quad (9)$$

The result (4) is recovered at large distances $|z_{\pm}|/a \gg 1$. At smaller distances $|z_{\pm}|/a = O(1)$, two discrepancies arise. First, all the wavenumber vectors satisfying the dispersion relation contribute to the wave field, instead of only those, of azimuthal angle $\varphi_k = \varphi$, associated with group velocity vectors pointing towards the point of observation. Secondly, the viscous and unsteady cutoffs involve the projected vertical distance $|z|/\cos \theta$, instead of the longitudinal distance $|z_{\pm}|$ along rays. Since $|z|/\cos \theta = |z_{\pm} \mp x_{\pm} \tan \theta|$, a transverse asymmetry of the wave beams follows, the waves being more attenuated for $x_{\pm} < 0$ than for $x_{\pm} > 0$.

3.2 Added-mass effects

The representation of a rigid sphere of radius a oscillating at the velocity \mathbf{U} in a stratified fluid can be determined exactly (Voisin, 2007b). The result is the same (6) as in a homogenous fluid,

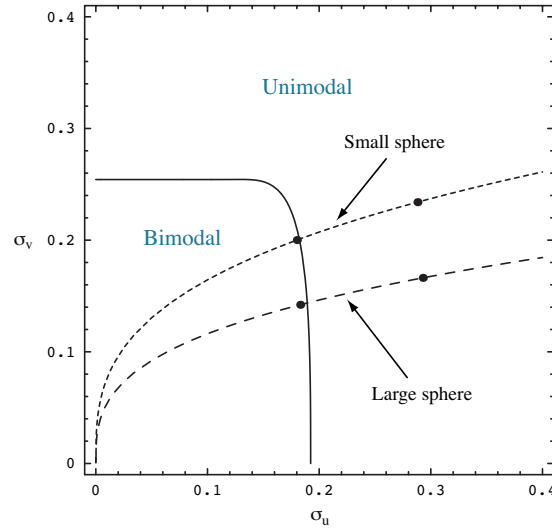


FIG. 2 – Regimes of internal wave propagation in the experiments of Flynn et al. (2003). The dashed curves represent the trajectories, in the (σ_u, σ_v) -plane, of each experiment as the distance from the oscillating sphere varies, and the points represent the positions at which the transverse profiles are plotted in figure 3.

except for the replacement of the actual velocity \mathbf{U} by the virtual velocity \mathbf{U}^* , of horizontal and vertical components

$$\mathbf{U}_h^* = \frac{4/3}{1 + B(\omega/N)} \mathbf{U}_h \quad \text{and} \quad W^* = \frac{2/3}{1 - B(\omega/N)} W, \quad (10)$$

varying with frequency according to

$$B\left(\frac{\omega}{N}\right) = \frac{\omega^2}{N^2} \left[1 - \left(1 - \frac{\omega^2}{N^2}\right)^{1/2} \left(i\frac{\pi}{2} + \operatorname{arccosh} \frac{N}{\omega} \right) \right]. \quad (11)$$

The physical interpretation of this result is a modification of the added mass of the sphere by the stratification, a phenomenon first noticed theoretically by Lai and Lee (1981) and verified experimentally by Ermanyuk and Gavrilov (2003). It is only in the limit $\omega \gg N$ that $B \rightarrow 1/3$ and $\mathbf{U}^* \rightarrow \mathbf{U}$, irrespective of the amplitude of oscillation.

4 Comparison with experiment

We apply the above results to the experiments of Flynn et al. (2003), involving two spheres, one small (such that $Re = 350$) and the other large (such that $Re = 1000$). The perturbation ΔN^2 of the squared buoyancy frequency is measured, and its amplitude $|\Delta N^2|$ is obtained by sampling the measurement at sixteen equally spaced times between the start $\omega t = 4\pi$ and the end $\omega t = 6\pi$ of the third period of oscillation, then calculating the root-mean-square average of the samples and multiplying the result by $\sqrt{2}$.

The theoretical perturbation is, for $\omega t \gg 1$ and $Re \gg 1$,

$$\Delta N^2 \sim \pm i N^2 \frac{A (\sin \theta \cos \theta)^2}{a (1 - B(\cos \theta))} \int_0^{(a \cos \theta)/(\alpha |z|)} \exp\left(-\frac{\beta |z|}{a^3 \cos \theta} K^3\right) \times K^2 j_1(K) J_0\left(K \frac{r_h}{a} \cos \theta\right) \exp\left(\mp i K \frac{z}{a} \sin \theta\right) dK, \quad (12)$$

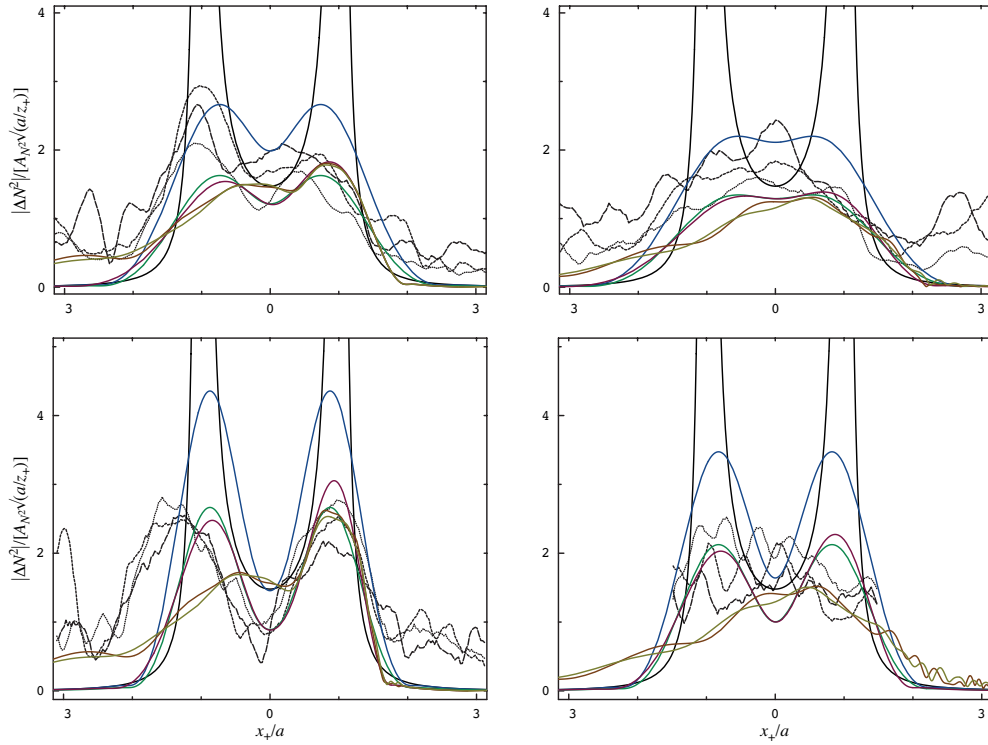


FIG. 3 – Transverse profiles of $|\Delta N^2|$ at two distances $z_+/a = 5$ (left) and 8 (right) from the small (top) and large (bottom) spheres in the experiments of Flynn et al. (2003). The dashed curves represent the experimental data for three oscillation amplitudes. The continuous curves represent the theory, starting from the steady inviscid far field (—) and adding cumulatively the effects of viscosity (—), added mass (—), near field (—), unsteadiness (—) and rms (—). The unsteady profiles are calculated at $\omega t = 5\pi$, and the rms profiles are deduced from sixteen samples starting at $\omega t = 4\pi$ and separated by $\pi/8$.

becoming, in the far field $|z_{\pm}| \gg a$,

$$\Delta N^2 \sim \pm \frac{e^{i\pi/4}}{\sqrt{2\pi}} N^2 \frac{A}{a} \frac{(\sin\theta \cos\theta)^{3/2}}{1 - B(\cos\theta)} \sqrt{\frac{a}{|z_{\pm}|}} \times \int_0^{a/(\alpha|z_{\pm}|)} \exp\left(-\frac{\beta|z_{\pm}|}{a^3} K^3\right) K^{3/2} j_1(K) \exp\left(iK \frac{x_{\pm}}{a}\right) dK. \quad (13)$$

Based on this far field, the bimodal and unimodal regimes are as represented in figure 2.

We focus in figures 3 and 4 on comparison with figures 8–11 of Flynn et al. (2003), where the amplitude is normalized by $A_{N^2} = (N^2/2)(A/a) \sin\theta \cos\theta$. The distinctive influence of each mechanism is visible in the theoretical curves: viscosity, smoothing out the inviscid singularities; added mass, diminishing the amplitude by 40%; near field, breaking the symmetry of the profiles; unsteadiness, adding oscillations. In the experimental curves, the dominant effect appears to be the added mass correction, especially for the large sphere. On top of it, an asymmetry is observed in the transverse profile for the small sphere at $z_+/a = 5$, but this asymmetry goes opposite to that predicted for near-field effects and is absent for the large sphere. The overall noise level of the measurements makes it difficult to assess unsteady effects precisely. These effects, though, seem to provide an explanation for the otherwise unexplained increase of the amplitude at sufficiently large z_+ for the large sphere on the axis $x_+ = 0$.

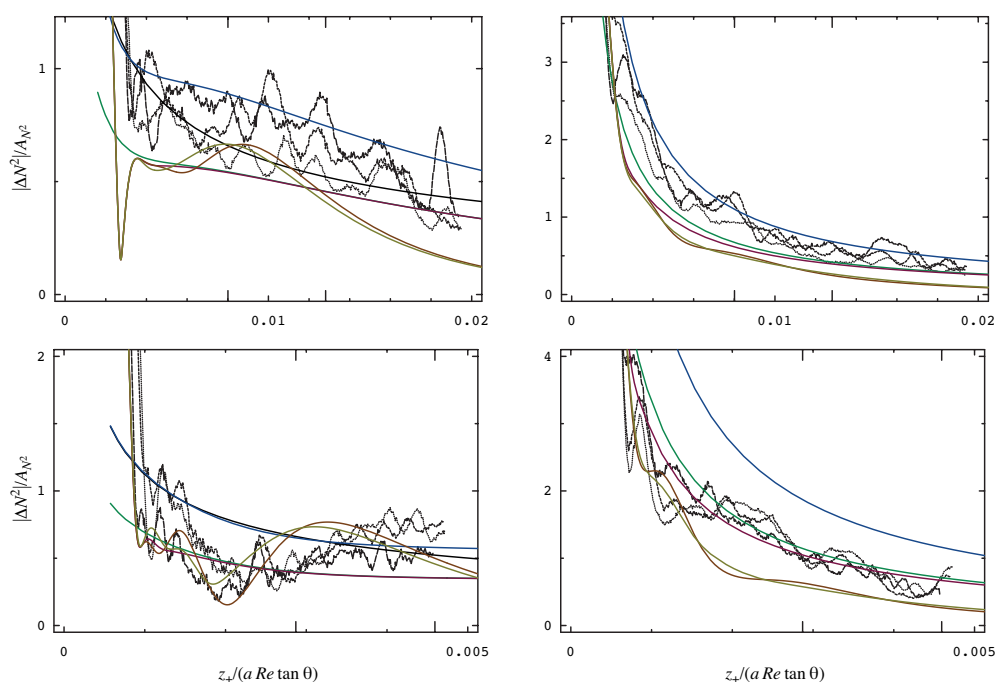


FIG. 4 – Longitudinal variations of $|\Delta N^2|$ at two positions $x_+/a = 0$ (left) and -1 (right) across the wave beam for the small (top) and large (bottom) spheres in the experiments of Flynn et al. (2003). The mode of representation is the same as in figure 3. The longer tick marks represent the positions $z_+/a = 5$ and 8 of the transverse profiles in figure 3.

References

- Dalziel, S.B., Hughes, G.O. & Sutherland, B.R. 2000 *Exps. Fluids* **28**, 322–335.
- Ermanyuk, E.V. & Gavrilov, N.V. 2003 *J. Fluid Mech.* **494**, 33–50.
- Flynn, M.R., Onu, K. & Sutherland, B.R. 2003 *J. Fluid Mech.* **494**, 65–93.
- Gorodtsov, V.A. & Teodorovich, E.V. 1986 *J. Appl. Mech. Tech. Phys.* **27**, 523–529.
- Lai, R.Y.S. & Lee, C.-M. 1981 *Int. J. Engng Sci.* **19**, 1411–1420.
- Lighthill, J. 1978 *Waves in Fluids*. Cambridge University Press.
- Makarov, S.A., Neklyudov, V.I. & Chashechkin, Yu.D. 1990 *Izv. Atmos. Ocean. Phys.* **26**, 548–554.
- Onu, K., Flynn, M.R. & Sutherland, B.R. 2003 *Exps. Fluids* **35**, 24–31.
- St. Laurent, L. & Garrett, C. 2002 *J. Phys. Oceanogr.* **32**, 2882–2899.
- Sutherland, B.R., Dalziel, S.B., Hughes, G.O. & Linden, P.F. 1999 *J. Fluid Mech.* **390**, 93–126.
- Voisin, B. 2003 *J. Fluid Mech.* **496**, 243–293.
- Voisin, B. 2007a Transition regimes of internal wave beams. (In preparation).
- Voisin, B. 2007b Oscillating bodies and added mass for motion in density-stratified fluids. (In preparation).